Red to Blue Tunable Upconversion in Tm^{3+}-Doped ZrO_2 Nanocrystals

Amitava Patra,*,† Pushpal Ghosh,† Paramita Saha Chowdhury,† Márcio A. R. C. Alencar,‡ Whualkuer Lozano B.,‡ Nikifor Rakov,§ and Glauco S. Maciel‡

Sol−Gel Division, Central Glass & Ceramic Research Institute, Jadavpur, Kolkata, 700 032, India, Departamento de Física, Universidade Federal de Pernambuco, 50670-901 Recife, PE, Brazil, and Universidade Federal do Vale do São Francisco, 56306-410 Petrolina, PE, Brazil

Received: February 8, 2005; In Final Form: March 23, 2005

The effect of dopant concentration on the blue upconversion (UPC) emission of Tm^{3+} -doped ZrO_2 nanocrystals under different excitation wavelengths in the red region is reported. The UPC emissions are due to the f−f electronic transitions from excited states $^1G_4$ and $^1D_2$ of Tm^{3+}. We observed a chromatic change in the UPC with tuning the excitation wavelength. The UPC emission bands at 475, 488, and 501 nm are observed under excitation at 649 nm, but bands centered at 454 and 460 nm are observed when the excitation wavelength is tuned to 655 nm. The UPC emission could be tuned from 501 to 454 nm (∼47 nm) by changing the excitation wavelength from 649 to 655 nm (∼6 nm). The pump power dependence of the emission bands at 475, 488, and 501 nm were investigated on excitation intensity at 649 nm, and the emission bands at 454 and 460 nm are investigated on excitation intensity at 655 nm, which confirms that all of these UPC emission lines are a two-photon absorption process.

1. Introduction

The research in the field of rare-earth doped nanocrystals for upconversion emission has recently been recognized to hold tremendous potential in the areas of photonic and biophotonic applications.[1−3] Intensive research efforts are therefore devoted to designing and tuning the upconversion properties of these materials. There are few reports on upconversion luminescence of trivalent-rare-earth ions doped nanocrystals.[4−11] Most recently, rare-earth doped nanocrystals in colloidal solution have also been reported.[12] Combining the promising optical properties of rare-earth (RE) ions due to small electron−phonon coupling strengths of the excited states and nanoparticles, the study of luminescence properties of RE ions in nanoscale environment is important. In case of RE ions doped in dielectric nanoparticles, luminescence may be achieved by inducing electronic f−f transitions, which involves electrons that are localized in atomic orbitals of the ions. Therefore, no size-dependent quantization effect (due to confinement of delocalized electrons) is found in these transitions. However, confinement effects may be induced by inter-ionic electronic interaction and, particularly, through electron−phonon interaction,[13] which has important manifestations in influencing the optical properties. A very broad range of unprecedented optical properties can be observed by changing the host lattice and dopant concentration. The efficiency of a RE-doped nanoparticle for frequency upconversion (UPC) of infrared radiation into shorter wavelengths is often influenced by changing the crystal structure of host due to change of phonon frequency of host and dopant concentration.[4−6] Among the oxide hosts, the zirconia matrix seems to be an ideal medium for preparation of highly luminescent materials because it is chemically and photochemically stable, has a high refractive index, and has a low phonon energy.[4] Studies of the upconversion process in thulium (Tm^{3+})-doped materials are of great interest because Tm^{3+} exhibits strong fluorescence in the violet and blue region.[14,15] The main goal of this work is to study the upconversion luminescence of Tm^{3+} in ZrO_2 matrix and the way it changes with concentration and excitation wavelength. From the fundamental point of view, the physical understanding of the upconversion process of rare-earth doped oxide nanocrystals and the way it changes with size, crystal phase, and concentration is very important. There is plenty of scope for understanding the effect of dopant concentration and the excitation wavelength on UPC luminescence efficiency of Tm^{3+}-doped ZrO_2 nanocrystals. To the best of our knowledge, there is no report on the study of blue UPC emission of Tm^{3+} doped in ZrO_2 nanocrystals and how this property changes with changing dopant concentration and the excitation wavelength.

Here, we have used the sol−emulsion−gel method to control the size and morphology of the nanoparticles, which we have already discussed in our previous studies.[4−6] In conventional methods, uncontrolled nucleation and subsequent growth of the precipitated particles in a bulk aqueous medium finally generates larger particles with a wide size distribution. The principle of this process involves the dispersion of a sol containing the desired constituents under agitation into a water-immiscible organic liquid for low dielectric constant. To stabilize the dispersed sol droplets, addition of an amphiphilic surface-active agent is necessary. Finally, gelation of the sol droplets with a suitable gelling agent produces gel particles.

Here, we report the influences of dopant concentration and excitation wavelength on the UPC luminescence properties of Tm^{3+}-doped ZrO_2 nanocrystals derived from the sol−emulsion−gel technique.

2. Experimental Procedure

The sol−emulsion−gel method is used for the preparation of Tm^{3+}-doped ZrO_2 nanoparticles. Zirconium propoxide

* Corresponding author. Fax: +91-33-24730957. E-mail: apatra@cgcri.res.in

† Central Glass & Ceramic Research Institute.

‡ Universidade Federal de Pernambuco.

§ Universidade Federal do Vale do São Francisco.

10.1021/jp050685v CCC: $30.25
Published on Web 04/28/2005

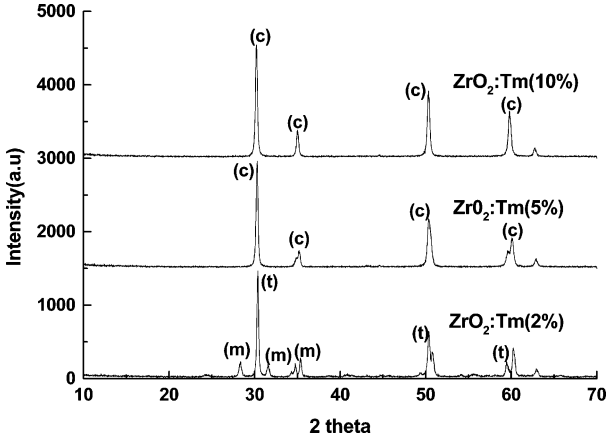

Figure 1. Powder X-ray diffraction patterns of different concentrations of Tm^{3+}-doped ZrO_2 nanocrystals prepared at 1000 °C.

(Fluka) and thulium acetate were used as the starting materials. First, 3 mL of glacial acetic acid was slowly added to 10 mL of zirconium propoxide and stirred for 30 min. Next, 20 mL of *n*-propanol was added to the solution, which was further stirred for 15 min at room temperature. Next, 4 mL of 50% aqueous acetic acid was slowly added to the above solution under stirring, which resulted in a clear transparent solution. The required (2.0, 5.0, and 10.0 mol % Tm_2O_3) amount of thulium acetate was then added to this solution. The emulsified sol droplets were obtained through water-in-oil (w/o) type emulsions with cyclohexane and sorbitan monooleate (Span 80, fluka) as the organic liquid (oil phase) and nonionic surfactant, respectively. The support solvent containing 5 vol % of span 80 in cyclohexane was used for emulsification, that is, for the preparation of the water-in-oil (w/o) type emulsion in the present study. The volume ratio of the sol and cyclohexane was 1: 4. A measured amount of thulium-doped zirconia sol was then dispersed in the solvent under stirring. The sol droplets formed in the process were then gelled by the controlled addition of a base. The gel particles were separated by centrifugation followed by washing with acetone and methanol. The product was dried at 60 °C and then heated at 1000 °C for 1 h. The crystalline phases of sintered powders were identified by X-ray diffraction (XRD). The crystallite sizes of the nanocrystals were calculated following Scherrer's equation:

$$D = K\lambda/\beta \cos \Theta \qquad (1)$$

where $K = 0.9$, D represents crystallite size (Å), λ is the wavelength of Cu kα radiation, and β is the corrected half width of the diffraction peak. We pressed the particles to form a smooth, opaque flat disk for optical study. Optical absorption was obtained using a Cary 300 (diffuse reflectance UV−vis). UPC experiments were performed using a CW dye laser that operates from 645 to 658 nm as the excitation source. The UPC luminescence was collected with a multimode fiber connected to a monochromator attached to a nitrogen-cooled CCD detector for spectral analysis. The UPC signal was sent to a personal computer for processing. The measurements were performed at room temperature.

3. Results and Discussion

3.1. Structural Investigations. The powder XRD patterns (Figure 1) show the presence of monoclinic, tetragonal, and cubic phases of different concentrations of Tm^{3+}-doped ZrO_2 nanocrystals obtained after heating at 1000 °C. For 2.0 mol % Tm^{3+}-doped ZrO_2 nanocrystals, two lines at 28.2° (1 1-1) and 31.4° (111) are observed for the monoclinic phase (m) (JCPDS 37 1484), and the calculated crystallite sizes from the above-mentioned peaks are 22.8 and 26.3 nm, respectively. The strongest line at 30.17° (111) is observed for the same sample, which is due to the metastable tetragonal phase (JCPDS 17 0923), and the calculated crystallite size from this peak is 36.22 nm. From XRD study, it shows that the tetragonal phase (t) is the dominant structure for 1000 °C annealed Tm^{3+} (2.0 mol %) ZrO_2 nanocrystals and the percentage of tetragonal phase is 81.3%. However, in case of 1000 °C annealed Tm^{3+} (5 and 10.0 mol %) ZrO_2 nanocrystals, the strong line 30.5° (111) for cubic phase (c) (JCPDS 27 0997) is obtained. The calculated crystal sizes (at 30.5°) are 30 and 32.8 nm for 5.0 and 10.0 mol % Tm-doped ZrO_2 nanocrystals, respectively. The diameter of rare-earth ion (M^{3+}) is larger than that of Zr^{4+}; therefore, the introduction of such ion will induce the change of ZrO_2 lattice. At low dopant concentrations, monoclinic structure of zirconia is observed with a space group of $P2_1/c$, where each Zr atom is in 7-fold coordination with oxygens. The crystal structure of tetragonal ZrO_2 is a body-centered lattice with the space group $P4_2/nmc$. It is well known that the stabilization of the fluorite-type zirconia lattice can be achieved by oxygen vacancies mechanism for trivalent dopants. However, at higher concentration (5.0 and 10.0 mol % Tm), the cubic phase is obtained with the space group $Fm3m$. These results clearly indicate the crystal structure and crystal symmetry depend on the concentration of dopant ions. This result clearly shows how the crystal phase and their composition can be controlled by changing the Tm^{3+} concentration at a fixed temperature of heating.

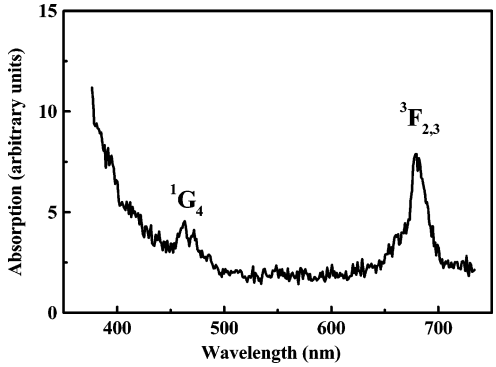

Figure 2. The absorption spectrum of 10.0 mol % Tm^{3+}-doped ZrO_2 nanocrystals prepared at 1000 °C.

3.2. Upconversion Properties. Figure 2 shows the typical absorption spectrum of 10.0 mol % Tm^{3+}-doped ZrO_2 nanocrystals heat-treated at 1000 °C. The bands peaked at 463 and 680 nm are due to the ground-state ($^3H_6$) electronic transitions to levels $^1G_4$ and $^3F_{2,3}$, respectively. Figure 3 depicts the UPC luminescence of different concentrations of Tm^{3+}-doped ZrO_2 nanocrystals prepared at 1000 °C under excitation at 649 nm. We measure the UPC luminescence under identical condition to compare their emission efficiency. The UPC emission bands centered at 475, 488, and 501 nm are assigned to the $^1G_4 \rightarrow {}^3H_6$ transition. From XRD study, it is seen that tetragonal and monoclinic phases are present in 2.0 mol % Tm-doped ZrO_2 sample prepared at 1000 °C. The crystal field effect in this nanocrystal is the main reason to split this $^1G_4 \rightarrow {}^3H_6$ transition band into three bands. It is well known that the f−f transition is very narrow and exhibits multiple structures derived from electronic interactions, as well as spin−orbit coupling. Therefore, the splitting of the Tm-4f shell is due to the crystal field. Again, it is reported[16] that the presence of yttrium provides a reduction of the effective coordination of zirconium by oxygen

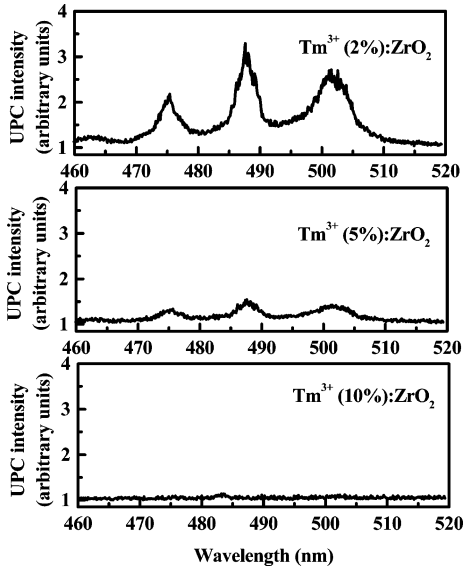

Figure 3. The UPC luminescence of different concentrations of Tm^{3+}-doped ZrO_2 nanocrystals prepared at 1000 °C under excitation at 649 nm. Laser power: 270 mW.

from 8-fold to 7-fold by introduction of additional Y 4p valence bands and Y 4d conduction bands. We have already reported the influences of dopant concentration on the crystal structure and their overall crystal field effects on Er^{3+} ions in ZrO_2 nanocrystals.[17] Figure 3 shows that very low luminescence intensity is observed for 5.0 mol % Tm^{3+}-doped ZrO_2 nanocrystals prepared at 1000 °C and no UPC emission is observed for 10.0 mol % Tm^{3+}-doped ZrO_2 nanocrystals prepared at the same temperature, measured under identical conditions. It is clearly seen that the intensities of these bands increase with decreasing the concentration of Tm^{3+} in our samples. This clearly indicates that the dopant concentration has a strong effect on luminescence efficiency of Tm^{3+}-doped ZrO_2 nanocrystals. It is known that the ions in low concentration are usually randomly distributed in the host lattice and the distances are too far apart, but at higher concentration, the distances between two ions are shortened, thus leading to formation of pairs. Here, at low concentration (2.0 mol %, Tm), the mean distance (R) between the Tm^{3+} ions is estimated by $R = 0.62/(N)^{1/3}$ (where N is the concentration of ions), but the distance between the Tm^{3+} ions-doped ZrO_2 nanocrystals are 0.91, 0.67, and 0.53 nm for 2.0, 5.0, and 10.0 mol % Tm^{3+} ions concentration, respectively.[18] Therefore, at high concentration, the ions can interact by electric multipolar process leading to energy migration and concentration quenching of fluorescence. The dipole−dipole quenching process is inversely proportional to the sixth power of the ion−ion separation and thus to the square of the Tm^{3+}-concentration. In the case of higher concentration of Tm^{3+} ions, the cross relaxation process occurs followed by nonradiative decay of the two ions to the ground state. Therefore, we can say that concentration of Tm^{3+} ions has also played an important role in the upconversion emission efficiency of Tm^{3+}-doped ZrO_2 nanocrystals.

A dramatic change in the UPC of Tm^{3+} has been observed by changing the pumping wavelength. Figure 4 shows the upconversion emission spectra of 2.0 mol % Tm^{3+}-doped ZrO_2 nanocrystals prepared at 1000 °C. The upconversion emission bands at 475, 488, and 501 nm are observed under excitation at 649 nm, but bands centered at 454 and 460 nm are observed when the excitation wavelength is tuned to 655 nm (the same pump intensity was used for both excitation wavelengths). The bands at 454 and 460 nm are due to the $^1D_2 \rightarrow {}^3H_5$ transition.

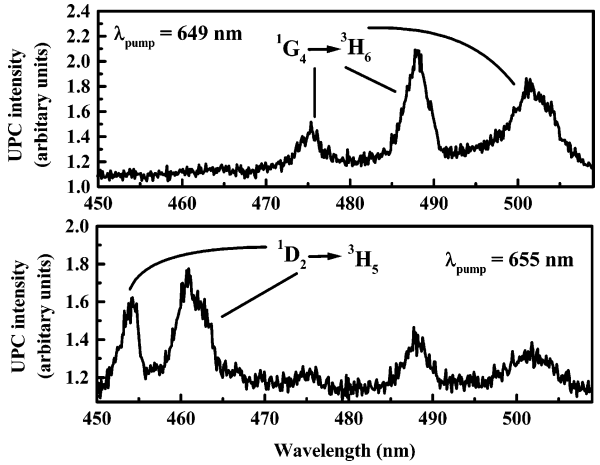

Figure 4. The UPC luminescence of 2.0 mol % Tm^{3+}-doped ZrO_2 nanocrystals prepared at 1000 °C under excitation at 649 and 655 nm. Laser power: 270 mW.

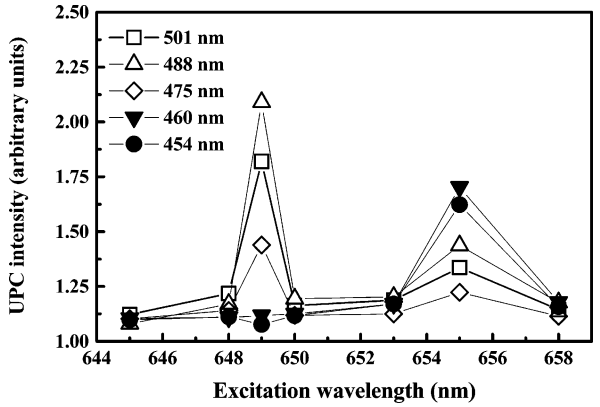

Figure 5. The UPC emission intensity change with the excitation wavelength for the five main peaks. Laser power: 270 mW.

This upconversion chromaticity phenomenon is an important observation in this study. Therefore, the tuning of pumping wavelength gives a very broad range of possibilities in the development of compounds with new and unprecedented upconversion properties in Tm^{3+}-doped ZrO_2 nanocrystals. These results show how the upconversion emission can be tuned by changing the wavelength of excitation. The broad range of tunability (the UPC emission can be tuned by ∼53 nm by changing the excitation wavelength by ∼6 nm) may be associated, for example, to the different site symmetries of dopant ions, which produces large inhomogeneous broadening of electronic forced dipole transitions (EFDPs). EFDPs of rare-earth ions are strongly affected by the local field symmetry and coupling strength with the host matrix. As a consequence, inhomogeneous broadening of such transitions increases with local asymmetry and/or matrix disorder. To prove this analysis, a more systematic study must be carried out, for example, in samples of different host materials with the same size and doped with the same rare-earth ion concentration. Figure 5 shows the UPC emission change with the excitation wavelength for the five main peaks observed in Figure 4. Note that the emission $^1G_4 \rightarrow {}^3H_6$ is stronger at 649 nm excitation wavelength, while the emission $^1D_2 \rightarrow {}^3H_5$ dominates at 655 nm excitation wavelength. This is because by changing the excitation wavelength it is possible to probe resonances of excited-state transitions involved in multiphoton absorption processes involved in producing UPC emission. The mechanisms responsible for the UPC processes observed in our samples are shown in Figure 6 with the help of energy level diagram. First, excitation

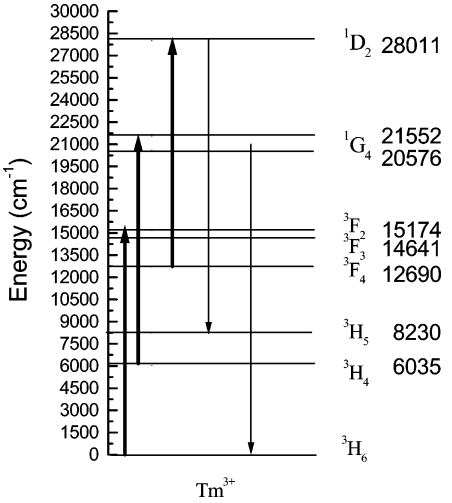

Figure 6. The energy level diagram for Tm^{3+} ions under excitation.

photons in the region of 650−700 nm can be absorbed because these excitation wavelengths match with the absorption transition between the ground state ($^3H_6$) and the excited levels ($^3F_{2,3}$) of Tm^{3+} as shown in Figures 2 and 6. After that, the population at excited states $^3F_{2,3}$ may decay to lower lying levels by emitting low energy photons (down conversion) or by nonradiative decay (activating optical phonon modes in the host lattice). Lower lying energy levels such as $^3H_4$ and $^3F_4$ may absorb excitation photons in the region of 650−700 nm and populate higher lying levels such as $^1G_4$ and $^1D_2$, respectively, as shown in Figure 6. Figure 5 shows that if the excitation wavelength is tuned to 649 nm (15 408 cm^{-1}), excited-state transition $^3H_4 \rightarrow {}^1G_4$ is favored. When the excitation wavelength is tuned to 655 nm (15 267 cm^{-1}), excited-state transition $^3F_4 \rightarrow {}^1D_2$ dominates. After level $^1G_4$ is populated, the UPC emission bands at 475, 488, and 501 nm are observed from the transition $^1G_4 \rightarrow {}^3H_6$. In case of level $^1D_2$, the UPC emission bands at 454 and 460 nm take place from the transition $^1D_2 \rightarrow {}^3H_5$. It is well known for an unsaturated mechanism that the intensity of the upconverted luminescence, I_{upc}, is proportional to some power n of the excitation intensity I_i, that is, $I_{upc} \propto I_i^n$, where $n = 2, 3, ...$ is the number of pump photons required to populate the emitting state and is determined from the slope of the line of the graph of intensity versus pump power in a log−log plot. To analyze the UPC mechanism which populates the $^1G_4$ level, the pump power dependence of the emission from $^1G_4 \rightarrow {}^3H_6$ level at 475, 488, and 501 nm was investigated on excitation intensity at 649 nm for 2.0 mol % Tm^{3+}-doped ZrO_2 nanocrystals prepared at 1000 °C, and the results are shown in Figure 7a. The experimental data have been fit with a straight line with slope of ∼2 (quadratic), which indicates that the blue UPC emission from Tm^{3+} is a two-photon process for all three emission bands. The pump power dependence of the emission bands at 454 and 460 nm was investigated on excitation intensity at 655 nm, and the result is shown in Figure 7b. The experimental data for 460 and 454 nm emission bands have been fit with a straight line with a slope of ∼2, which confirms that these UPC emission lines are also a two-photon absorption process.

4. Conclusions

Results indicate that chemical synthesis through the sol−emulsion−gel method is an excellent route for the preparation of Tm^{3+}-doped ZrO_2 nanocrystals. We have shown that the crystal structure and site symmetry can be changed by controlling the Tm^{3+} concentration. The upconversion emission bands at 475, 488, and 501 nm are observed under excitation at 649 nm, but bands centered at 454 and 460 nm are observed when the excitation wavelength is tuned to 655 nm. Our results highlight the importance of the role of dopant concentration and excitation wavelength on upconverted luminescence property of Tm^{3+}-doped ZrO_2 nanocrystals. We observed a chromatic change in the UPC with tuning the excitation wavelength. The pump power dependence of the emission bands at 475, 488, and 501 nm is observed under excitation at 649 nm, and the emission bands at 454 and 460 nm are investigated on excitation intensity at 655 nm, which confirms that these UPC emission lines are a two-photon absorption process. In conclusion, we must say that the judicious choice of dopant concentration of Tm^{3+} ions and excitation wavelength have played a major role on the tunable blue UPC emission in Tm^{3+}-doped ZrO_2 nanocrystals.

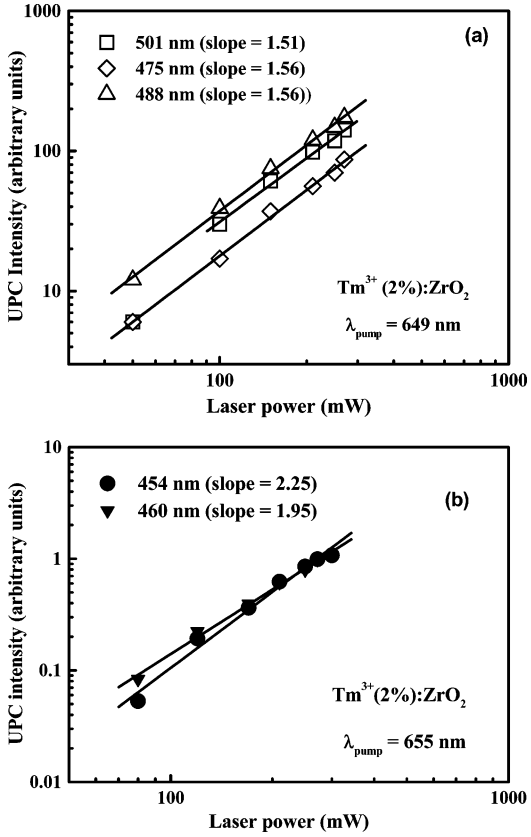

Figure 7. (a) The pump power dependence of the emission intensity from $^1G_4 \rightarrow {}^3H_6$ at 475, 488, and 501 nm investigated on excitation at 649 nm for 2.0 mol % Tm^{3+}-doped ZrO_2 nanocrystals prepared at 1000 °C. (b) The pump power dependence of the emission intensity from $^1D_2 \rightarrow {}^3H_5$ at 454 and 460 nm investigated on excitation at 655 nm for 2.0 mol % Tm^{3+}-doped ZrO_2 nanocrystals prepared at 1000 °C.

Acknowledgment. A.P., P.G., and P.S.C. thank Dr. H. S. Maiti, Director of CGCRI, for his constant encouragement and active cooperation in carrying out this work. They acknowledge the financial support by the Department of Science and Technology (NSTI, No. SR/S5/NM-05/2003). G.S.M. acknowledges A. S. L. Gomes (Universidade Federal de Pernambuco) for sharing the equipment used in the UPC experiments and the Brazilian agency Conselho Nacional de Desenvolvimento Ciêntífico e Tecnológico (CNPq) for financial support. W.L.B. acknowledges the financial support of Centro Latinoamericano de Fisica (CLAF).

References and Notes

(1) Prasad, P. N. *Nanophotonics*; John Wiley & Sons: New York, 2004.
(2) Silversmith, A. J.; Lenth, W.; Macfarlane, R. M. *Appl. Phys. Lett*. **1987**, *51*, 1977.
(3) Niedba, A. R. S.; Feindt, H.; Kordos, K.; Vail, T.; Burton, J.; Bielska, B.; Li, S.; Milunic, D.; Bourdelle, P.; Vallejo, R. *Anal. Biochem*. **2001**, *293*, 22.
(4) Patra, A.; Friend, C. S.; Kapoor, R.; Prasad, P. N. *J. Phys. Chem. B* **2002**, *106*, 1909.
(5) Patra, A.; Friend, C. S.; Kapoor, R.; Prasad, P. N. *Chem. Mater*. **2003**, *15*, 3650.
(6) Patra, A.; Friend, C. S.; Kapoor, R.; Prasad, P. N. *Appl. Phys. Lett*. **2003**, *83*, 284.
(7) Alencar, M. A. R. C.; Maciel, G. S.; de Araújo, C. B.; Patra, A. *Appl. Phys. Lett*. **2004**, *84*, 4753.
(8) Chen, W.; Joly, A. G.; Zhang, J. Z. *Phys. Rev. B* **2001**, *64*, 041202.
(9) Capobianco, J. A.; Vetrone, F.; Boyer, J. C.; Speghini, A.; Bettinelli, M. *J. Phys. Chem. B* **2002**, *106*, 1181.
(10) Matsuura, D. *Appl. Phys. Lett.* **2002**, *81*, 4526.
(11) Rosa-Cruz, E. De La.; Diaz-Torres, L. A.; Rodriguez-Rojas, R. A.; Meneses-Nava, M. A.; Barbosa-Garcia, O.; Salas, P. *Appl. Phys. Lett.* **2003**, *83*, 4903.
(12) Heer, S.; Lehmann, O.; Haase, M.; Gudel, H. U. *Angew. Chem., Int. Ed.* **2003**, *42*, 3179.
(13) Meltzer, R. S.; Hong, K. S. *Phys. Rev. B* **2000**, *61*, 3396.
(14) Rakov, N.; Macial, G. S.; Sundheimer, M. L.; Menezes, L. De S.; Gomes, A. S. L.; Messaddeq, Y.; Cassanjes, F. C.; Poirier, G.; Ribeiro, S. J. L. *J. Appl. Phys.* **2002**, *92*, 6337.
(15) Otto, A. P.; Brewer, K. S.; Silversmith, A. J. *J. Non-Cryst. Solids* **2000**, *265*, 176.
(16) French, R. H.; Glass, S. J.; Ohuchi, F. S.; Xu, Y. N.; Ching, W. Y. *Phys. Rev. B* **1994**, *49*, 5133.
(17) Patra, A. *Chem. Phys. Lett.* **2004**, *387*, 35.
(18) Chen, C. Y.; Petrin, R. R.; Cyeh, D.; Sibley, W. A. *Opt. Lett*. **1989**, *14*, 432.